Draheim et al., http://www.jcb.org/cgi/content/full/jcb.201407129/DC1

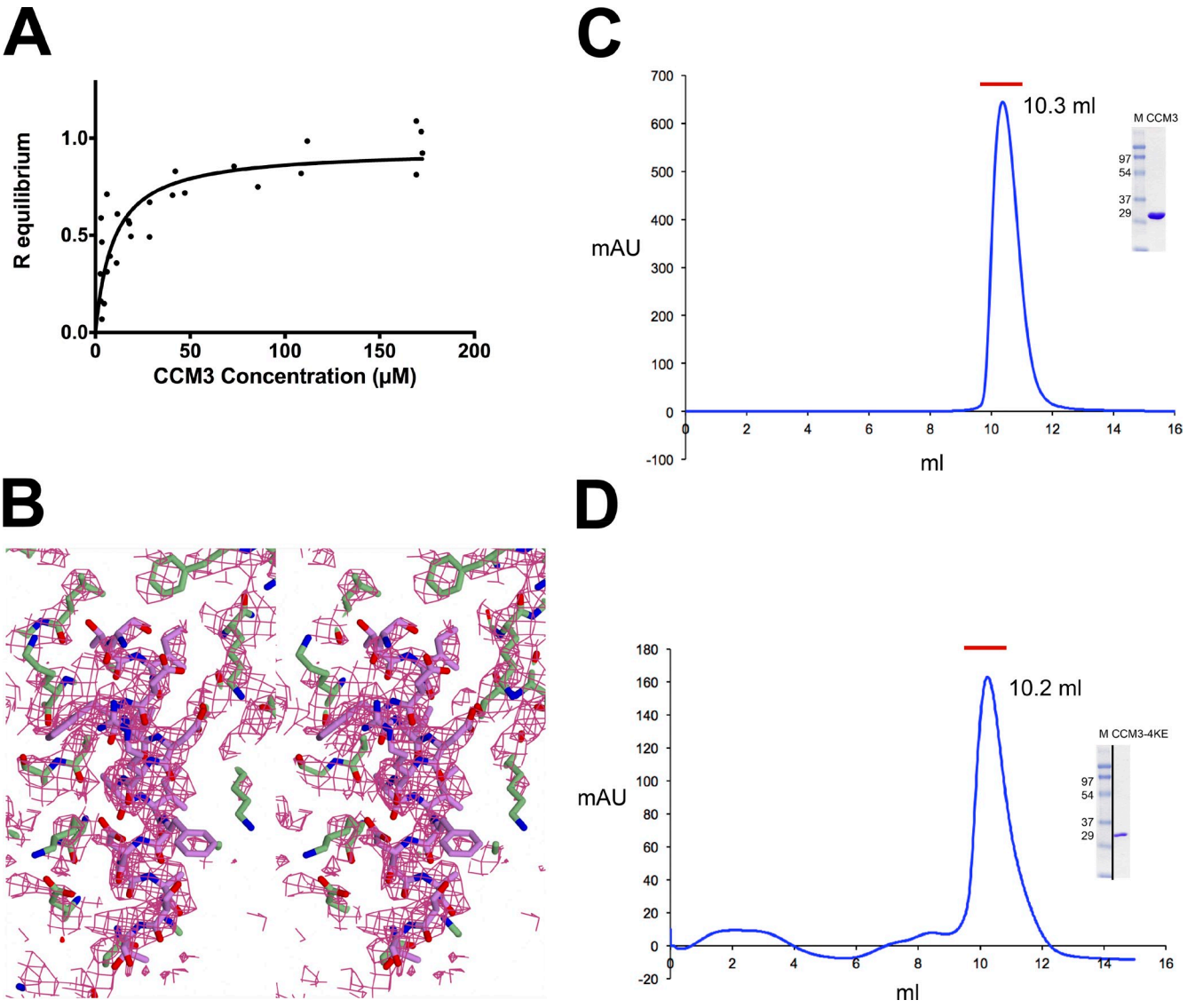

Figure S1. **Biolayer interferometry, simulated annealing omit map, and size exclusion chromatography.** (A) Affinity determination for CCM2 LD binding to CCM3 by biolayer interferometry. K_d was calculated with one-site saturation binding curve fitting using R equilibrium and CCM3 concentration. Value is determined to be 9.5 ± 2.5 μM. There are a total of 27 data points from three dilution series. (B) A stereoview simulated annealing omit map calculated using Phenix is shown in purple at 1σ. N and C termini of CCM2 LD peptide are shown. CCM2 is shown in purple, CCM3 in green. (C and D) Size exclusion chromatography (S75 column; GE Healthcare) and SDS-PAGE of elution peak for wild-type CCM3 (C) and CCM3^{4KE} (D). Chromatographs are representative of five independent purifications of wild-type CCM3 and one purification of CCM3^{4KE}. The black line indicates a break in the gel.

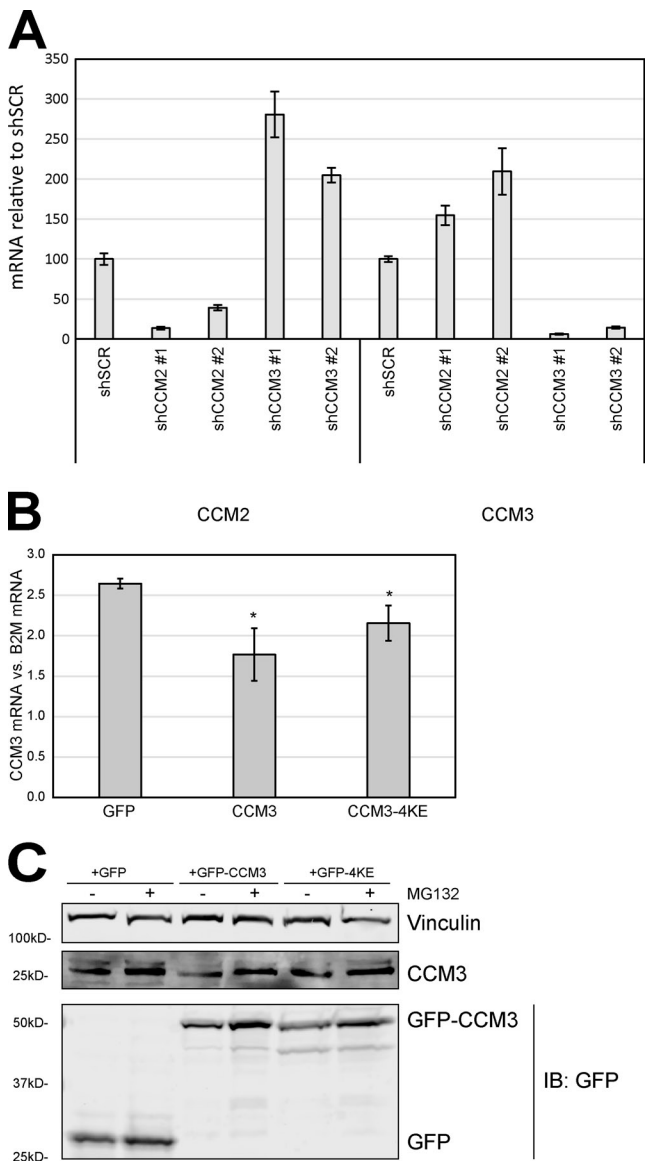

Figure S2. **qPCR analysis of CCM2 or CCM3 knockdown cells and qPCR analysis and proteasome inhibition of cells overexpressing CCM3.** (A) RNA isolated from CCM2 and CCM3 knockdown cell lines was analyzed for *CCM2* and *CCM3* levels using qPCR. The bar chart represents the relative (vs. shSCR) expression levels once normalized to loading control B2M. Data are mean ± SEM (error bars) from three experiments. (B and C) Exogenous expression of CCM3 leads to decreased *CCM3* levels and proteasome-dependent degradation of endogenous protein. (B) RNA isolated from EA.hy926 cells stably expressing either GFP, GFP-CCM3, or GFP-CCM3-4KE was analyzed for endogenous *CCM3* using real-time PCR (primers only recognize UTR). Error bars indicate SEM. (C) EA.hy926 cells stably expressing GFP, GFP-CCM3, or GFP-CCM3-4KE were treated with proteasome inhibitor MG132 or DMSO. Lysates from the treated cells were immunoblotted for endogenous CCM3.

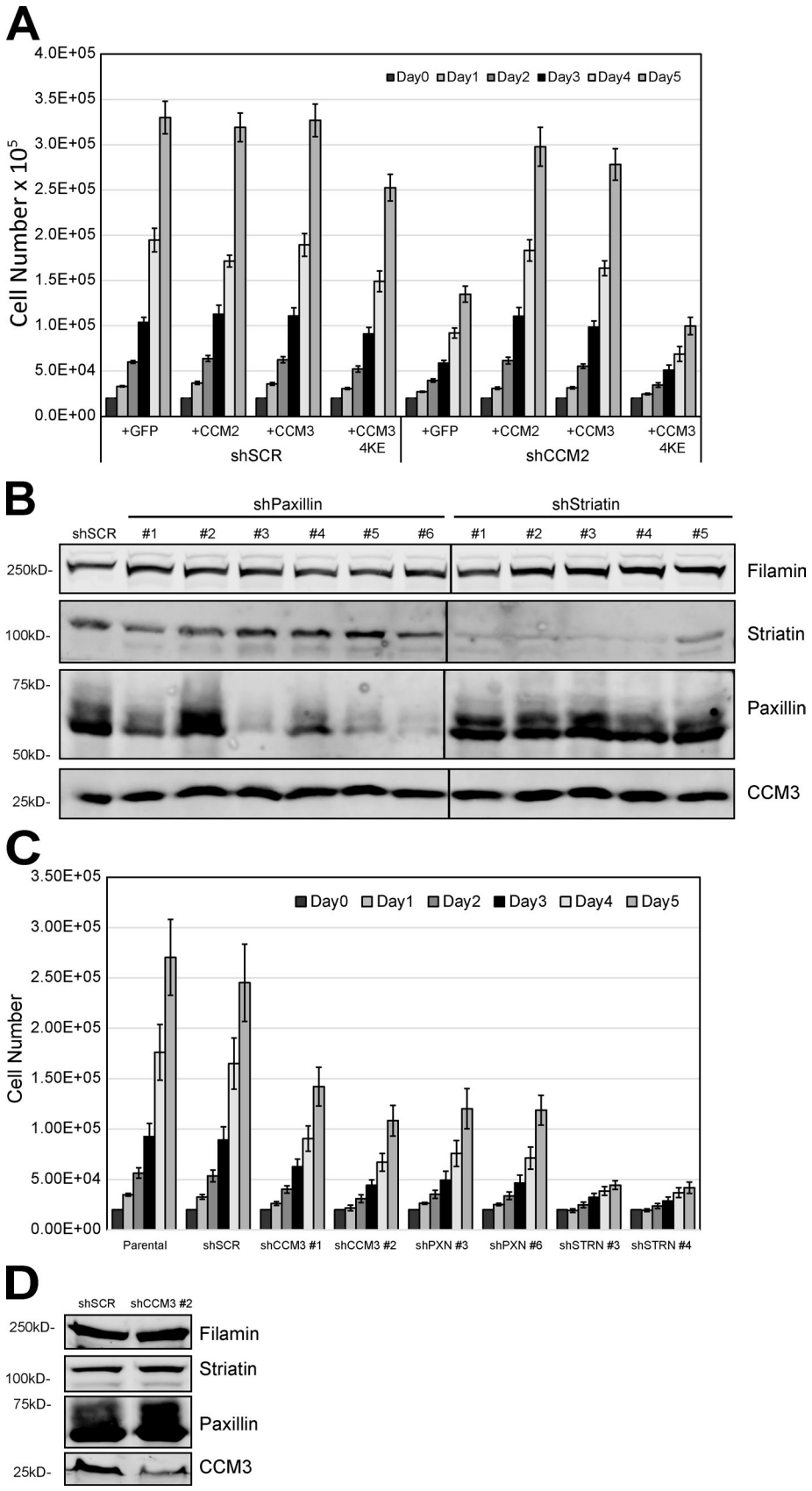

Figure S3. **Loss of CCM3 binding partners Striatin or Paxillin leads to defects in cell growth, but does not affect CCM3 expression.** (A) The effects of stably expressing GFP, GFP-CCM2, GFP-CCM3, and GFP-CCM3^{4KE} in stable control (shSCR) and CCM2 knockdown (shCCM2 #1) EA.hy926 cells were evaluated in a 5-d growth assay. The mean cell number ± SEM (error bars) from at least nine experiments is plotted. (B) Immunoblotting of lysates from STRN or PXN knockdown EA.hy926 cells. EA.hy926 cells stably infected with control scrambled shRNA (shSCR) or with shRNAs against Paxillin (shPXN #1–6) or Striatin-1 (shSTRN #1–5) were lysed and expression was probed by immunoblotting. CCM3 levels were also evaluated, but remained unchanged. Vinculin was used as a loading control. (C) Stable PXN and STRN knockdown cells were evaluated for 5 d in a cell growth assay and compared with cells infected with a virus expressing a scrambled hairpin and CCM3 knockdown cells. The bar graph reports the mean cell number ± SEM (error bars) from at least nine experiments. (D) Expression of vinculin (loading control), striatin, paxillin, and CCM3 in shSCR control cells and CCM3 knockdown cells was assessed by immunoblotting.

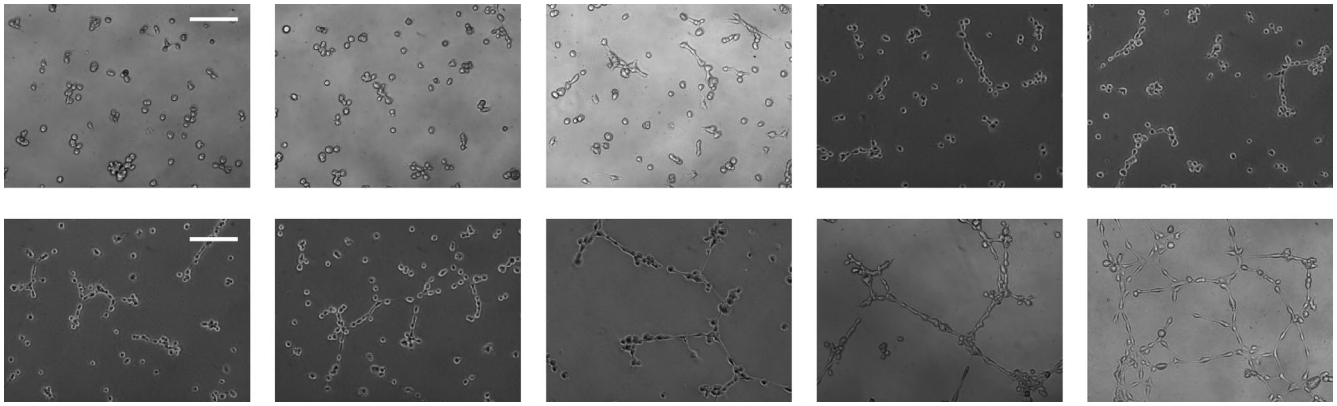

Figure S4. **Variability in network formation in CCM2 knockdown cells rescued with GFP-CCM2$^{LI/RR}$.** Representative images of networks formed by CCM2 knockdown EA.hy926 lines reexpressing GFP-CCM2$^{LI/RR}$.

Table S1. **Comparison of apparent binding affinities for FAT or FAT-H domains with LD motifs**

Protein	LD motif	Technique	Apparent K_d
CCM3	CCM2^{LD}	Pull-down	8.6 µM
	CCM2^{LD}	BLI	9.5 µM
	CCM2^{FL}	Pull-down	8.8 µM
	Paxillin-LD1	SPR	17 µM
	Paxillin-LD2	SPR	39 µM
	Paxillin-LD4	SPR	23 µM
FAK	Paxillin-LD2	ITC	9–11.5 µM
	Paxillin-LD4	NMR	25.3 µM
Pyk2	Paxillin-LD2	ITC	45 µM
GIT1	Paxillin-LD4	ITC	10 µM
	Paxillin-LD2	SPR	25 µM
	Paxillin-LD4	SPR	7 µM

Citations: CCM3–paxillin interactions (Li et al., 2011), FAK–paxillin (Gao et al., 2004), Pyk2–paxillin (Gao et al., 2004), GIT1–paxillin (Schmalzigaug et al., 2007; Zhang et al., 2008). SPR, surface plasmon resonance; ITC, isothermal titration calorimetry; NMR, nuclear magnetic resonance; BLI, biolayer interferometry.

Table S2. **Data collection and refinement statistics**

Criterion	Value
Data collection	
x-ray source	NSLS X25
Space group	$P2_12_12_1$
Wavelength (Å)	1.1000
Cell dimensions	
a, b, c (Å)	61.9, 113.6, 120.0
α, β, γ (°)	90, 90, 90
Resolution range (Å)	50.0–2.8 (2.9–2.8) [3.15–3.02]
No. of unique reflections	21,186
Completeness (%)	99.0 (97.5) [97.0]
R_{sym} (%)	10.7 (93.7) [58.3]
R_{pim}(%)	6.2 (38.8) [23.1]
$\langle I \rangle / \langle \sigma(I) \rangle$	16.0 (1.6) [3.1]
Redundancy	6.2 (6.2) [6.2]
Wilson *B*-factor (Å^2)	78.9
Refinement	
Resolution range (Å)	49.5–2.8 (2.9–2.8)
R factor (%)	
Working set	23.9 (25.6)
Test set	27.7 (30.2)
Reflections (total)	21,136
Free *R* reflections (%)	5.09
Free *R* reflections, No.	1,076
Residues built (Total #)	735
Chain A (CCM3)	17–86, 108–133, 166–207
Chain B (CCM3)	12–93, 96–149, 161–209
Chain C (CCM3) and chain E (CCM2)	C: 1–86, 90–153, 156–210; E: 224–239
Chain D (CCM3)	15–87, 91–154, 157–210
No. non-hydrogen protein atoms	5,969
Mean *B*-factor (Å^2)	71.5
Model statistics	
R.M.S.D. bond lengths (Å)	0.002
R.M.S.D. bond angle (°)	0.583
Ramachandran plot (%)	
Favored / allowed / outliers	98.6/1.4/0.0
MolProbity score	
Score	1.49
Percentile	100th

Parentheses indicate statistics for the high-resolution shell, brackets indicate statistics for the shell where $\langle I \rangle / \langle \sigma(I) \rangle = 3$.

References

Gao, G., K.C. Prutzman, M.L. King, D.M. Scheswohl, E.F. DeRose, R.E. London, M.D. Schaller, and S.L. Campbell. 2004. NMR solution structure of the focal adhesion targeting domain of focal adhesion kinase in complex with a paxillin LD peptide: evidence for a two-site binding model. *J. Biol. Chem.* 279:8441–8451. http://dx.doi.org/10.1074/jbc.M309808200

Li, X., W. Ji, R. Zhang, E. Folta-Stogniew, W. Min, and T.J. Boggon. 2011. Molecular recognition of Leucine-Aspartate Repeat (LD) motifs by the FAT-homology domain of cerebral cavernous malformation 3 (CCM3). *J. Biol. Chem.* 286:26138–26147. http://dx.doi.org/10.1074/jbc.M110.211250

Schmalzigaug, R., M.L. Garron, J.T. Roseman, Y. Xing, C.E. Davidson, S.T. Arold, and R.T. Premont. 2007. GIT1 utilizes a focal adhesion targeting-homology domain to bind paxillin. *Cell. Signal.* 19:1733–1744. http://dx.doi.org/10.1016/j.cellsig.2007.03.010

Zhang, Z.M., J.A. Simmerman, C.D. Guibao, and J.J. Zheng. 2008. GIT1 paxillin-binding domain is a four-helix bundle, and it binds to both paxillin LD2 and LD4 motifs. *J. Biol. Chem.* 283:18685–18693. http://dx.doi.org/10.1074/jbc.M801274200